for lossy dielectric substrates, the theory developed in this paper has better accuracy and is clearly preferred.

In the results obtained for the microstrip and the coupled microstrip, the lowest order of accuracy, "zero order", was considered for the solutions. Nevertheless, it is not too difficult to achieve a higher degree of accuracy by increasing the order of the final matrix. This can be accomplished by simply expanding the currents or the fields in terms of appropriate basis functions like those, for instance, in [1].

The computer programs developed to generate the quoted results are in FORTRAN and are available by request.

ACKNOWLEDGMENT

The author wishes to thank Dr. J. B. Davies for his invaluable comments in the course of preparation of this paper.

REFERENCES

[1] D. Mirshekar-Syahkal, "Analysis of uniform and tapered transmission lines for microwave integrated circuits," Ph.D. thesis, University of London, London, England, 1979.
[2] R. A. Pucel, "Design consideration for monolithic microwave circuits," *IEEE Trans. Microwave Theory Tech.*, vol. MTT-29, pp. 513–534, June 1981.
[3] T. M Hyltin, "Microstrip transmission on semiconductor dielectrics," *IEEE Trans. Microwave Theory Tech.*, vol. MTT-13, pp. 777–781, Nov. 1965
[4] M. V Schneider, "Dielectric loss in integrated microwave circuits," *Bell Syst. Tech. J.*, vol. 48, pp. 2325–2332, Sept. 1969.
[5] T L. Simpson and B. Tseng, "Dielectric loss in microstrip lines," *IEEE Trans Microwave Theory Tech.*, vol. MTT-24, pp. 106–108, Feb 1976.
[6] M. Caulton, J. J. Hughes, and H. Sobol, "Measurement of the properties of microstrip transmission lines for microwave integrated circuits," *RCA Rev.*, vol. 27, pp 377–391, Sept. 1966.
[7] D. Mirshekar-Syahkal and J. B. Davies, "Accurate solutions of microstrip and coplanar structures for dispersion and for dielectric and conductor losses," *IEEE Trans. Microwave Theory Tech*, vol. MTT-27, pp. 694–699, July 1979.
[8] ———, "Computation of the shielded and coupled microstrip parameters in suspended and conventional form," *IEEE Microwave Theory Tech.*, vol. MTT-28, pp. 274–275, Mar 1980.
[9] T. Itoh and R Mittra, "A technique for computing dispersion characteristics of shielded microstrip lines," *IEEE Trans. Microwave Theory Tech.*, vol. MTT-22, pp. 896–898, Oct. 1974
[10] J. B Davies and D Mirshekar-Syahkal, "Spectral domain solution of arbitrary coplanar transmission line with multi-layer substrate," *IEEE Trans Microwave Theory Tech.*, vol. MTT-25, pp. 143–146, Feb 1977.
[11] D. E Muller, "A method for solving algebraic equations using an automatic computer," *Mathematical Tables and Other Aids to Computation*, vol. 10, pp. 208–215, 1956.
[12] E. Yamashita, "Variational method for the analysis of microstrip-like transmission lines," *IEEE Trans. Microwave Theory Tech.*, vol. MTT-16, pp. 529–535, Aug. 1968.
[13] M. V. Schneider, "Microstrip lines for microwave integrated circuits," *Bell Syst. Tech. J.*, vol. 48, no. 5, pp. 1421–1444, May–June 1969.

Mathematical Representation of Microwave Oscillator Characteristics by Use of the Rieke Diagram

KATSUMI FUKUMOTO, MASAMITSU NAKAJIMA, MEMBER, IEEE, AND JUN-ICHI IKENOUE

***Abstract*—This paper shows that the characteristics of oscillators can be phenomenologically expressed by a polynomial function of frequency and amplitude, provided the output signal is nearly sinusoidal, especially at microwave frequency. A method is presented of determining the coefficients of the polynomial from several points on the Rieke diagram, with two examples being shown. The characteristics of oscillators can consequently be represented by several parameters, as in the case of electron tubes and transistors, so that the design of an oscillator circuit may become easier with the aid of an electronic computer.**

Manuscript received December 16, 1982; revised June 17, 1983. This work was supported by a Grant from the Nippon Telegraph and Telephone Public Corporation, Japan

K. Fukumoto is with Semiconductor Research Laboratory, Sharp Corporation, Nara, Japan

M. Nakajima and J. Ikenoue are with Department of Electronics, Kyoto University, Kyoto, Japan.

I. INTRODUCTION

So far, extensive studies have been performed on oscillator characterization. An important contribution was made by van der Pol. Since then, almost all studies on oscillators have been based on his oscillator model. It appears, however, that few have investigated the oscillator model itself.

The purpose of this paper is to provide a new mathematical oscillator model. It will be shown that the nonlinear admittance of oscillators can be phenomenologically expressed by a polynomial function of frequency and amplitude, provided the output signal is nearly sinusoidal, especially at microwave frequency. A method is presented concerning how to determine the coefficients of the polynomial from several points on the Rieke diagram, and two examples will be shown. Although much time is consumed to draw diagrams, the Rieke diagram has so far been used to express the characteristics, especially of microwave oscillators [1], [2]. This is because the Rieke diagram has advantages since the equi-power and equi-frequency loci are geometrically plotted on the Smith chart, and since the load admittance is represented within a circle of finite extent.

In this paper, a mathematical expression of oscillator characteristics is proposed instead of the geometrical expression, so that the characteristics of oscillators may be represented by several parameters, as in the case of electron tubes and transistors. The design of oscillator circuits will then become easier with the aid of an electronic computer.

II. MATHEMATICAL EXPRESSION OF NONLINEAR ADMITTANCES

A. Van der Pol's Oscillator

Van der Pol gave a basic mathematical expression of oscillator characteristics allowing for nonlinearity. If his formulation is viewed from the standpoint of the fundamental oscillation frequency, the oscillator admittance can be represented by a function of frequency and voltage amplitude squared as [3]

$$Y(j\omega, |V|^2) = -G_0 + G_V|V|^2 + jB_\omega \Delta\omega \qquad (1)$$

where $\Delta\omega = \omega - \omega_0$, and ω_0 is the center frequency.[1] As is explained in the next section, the Rieke diagram of (1) is represented in the form of Fig. 2(b), while that of an existing oscillator is of Fig. 9. These two Rieke diagrams are different from each other chiefly in the following ways: i) Load locus on which maximum output power is generated is a circle in the case of van der Pol's oscillator, while an existing oscillator produces the maximum power at a single point on the Rieke diagram. ii) The Rieke diagram of van der Pol's oscillator is symmetric, while that of an existing oscillator is usually asymmetric.

B. Generalization of Oscillator Admittance

Fig. 1 shows an equivalent circuit of coupling of a microwave oscillator to a load. The effect of coupling strength of the

[1] The oscillation frequency when a matched load is connected to the line.

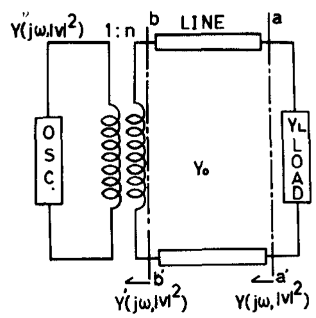

Fig. 1. Equivalent circuit of coupling of a microwave oscillator to a load.

oscillator to the transmission line is represented by an ideal transformer ($1:n$), so that we have

$$Y'(j\omega,|V|^2)=Y''(j\omega,|V|^2)/n^2. \tag{2}$$

This oscillator admittance is transformed by a line length

$$Y(j\omega,|V|^2)=\mathscr{L}\left[Y'(j\omega,|V|^2)\right]. \tag{3}$$

The transformation $\mathscr{L}$ means the counter-clockwise rotation of equi-power and equi-frequency loci on the Rieke diagram. Here we assume that the resultant admittance $Y(j\omega,|V|^2)$ is given by a polynomial function of frequency and voltage as given by

$$\begin{aligned}Y(j\omega,|V|^2)=&-G_0+jB_0+(G_\omega+jB_\omega)\Delta\omega\\&+(G_V+jB_V)|V|^2+(G_C+jB_C)\Delta\omega|V|^2\\&+(G_{\omega2}+jB_{\omega2})\Delta\omega^2.\end{aligned} \tag{4}$$

This is an extension of (1). Before we demonstrate that this model represents the characteristics of practical oscillators fairly well, we will investigate briefly the meaning of the coefficients of the variables $\Delta\omega$ and $|V|^2$.

In general, the first-order terms in $|V|$ may be included in the above equation. But, if they are included in addition to the second-order terms in $|V|$, the algebra is much more complicated; the load admittance that produces the maximum power cannot be expressed in closed form, as will be clear in the following. For IMPATT diodes, however, the replacement of $|V|$ for $|V|^2$ may give better results. In this case, the mathematics are not altered in substance.

Now, let the load admittance be $Y_L=G_L+jB_L$. By applying Kirchhoff's second law, we have

$$Y(j\omega,|V|^2)+Y_L=0. \tag{5}$$

The output power is given by

$$P=G_L|V|^2 \tag{6}$$

so that we have

$$Y(j\omega,P/G_L)+Y_L=0. \tag{7}$$

Normalizing (7) to the characteristic admittance Y_0 of the line gives the following equation:

$$Y(j\omega,P/G_L)/Y_0+Y_L/Y_0=\hat{Y}(j\omega,P/G_L)+\hat{Y}_L=0 \tag{8}$$

where the symbol $\hat{}$ denotes the normalization to Y_0. Plots of (8) on a Smith admittance chart, with ω or P kept constant, give the equi-frequency or equi-power loci on the Rieke diagram.

C. Stability Criterion

In this section, we consider the stability of solutions for (5). Assuming a small change $\delta|V|$ from the stationary voltage amplitude $|V_s|$ at frequency ω_s, we have a variational equation

$$\frac{1}{\delta|V|}\frac{d\,\delta|V|}{dt}=-\mathrm{Re}\left\{\frac{Y_{|V|}(j\omega_s,|V_s|^2)}{Y_{j\omega}(j\omega_s,|V_s|^2)}\right\}. \tag{9}$$

We see that $|V_s|$ is stable only when the right-hand side of (9) is negative [3], [4].

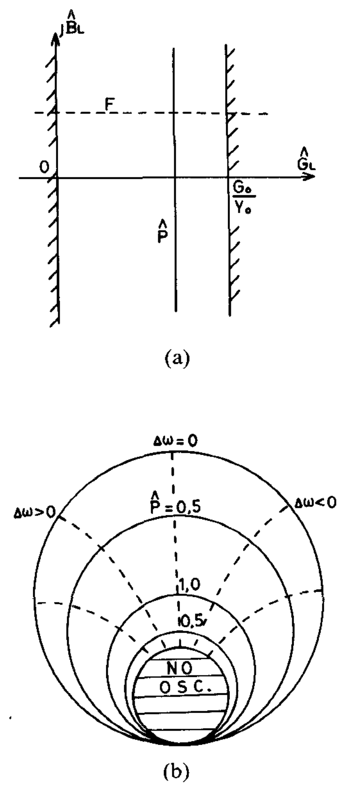

Fig. 2. van der Pol's oscillator. (a) Complex load plane. (b) Rieke diagram.

D. Meaning of Each Coefficient

We consider first the characteristics of van der Pol's oscillator as a basis. Maximum output power of van der Pol's oscillator is given by $P_m=G_0^2/4G_V$ (Appendix I). Let power P be normalized to P_m

$$\hat{P}=P/P_m=4G_VP/G_0^2. \tag{10}$$

Fig. 2(a) shows the equi-frequency and equi-power loci of van der Pol's oscillator on the complex load plane, and Fig. 2(b) represents those on the Smith chart. From the real part of (8), together with (10), the equi-power loci of van der Pol's oscillator may be written as (Appendix I)

$$\hat{G}_L=G_0\left(1\pm\sqrt{1-\hat{P}}\right)/2Y_0. \tag{11}$$

From (11), it is found that the maximum output power $\hat{P}=1$ is generated at every point on the admittance locus of $\hat{G}_L=G_0/2Y_0$. Equation (12) represents the equi-frequency locus

$$\hat{B}_L=-B_\omega\Delta\omega/Y_0 \tag{12}$$

with the central frequency line $\Delta\omega=0$, corresponding to the susceptance $\hat{B}_L=0$ line. It should be noted that the stability condition G_V, $B_\omega>0$ holds by applying (9).

1) Meaning of Coefficients G_ω and B_V: First of all, let us investigate the characteristics of an oscillator model containing two parameters G_ω and B_V in addition to van der Pol's oscillator model in (1). The equi-power and equi-frequency loci are respec-

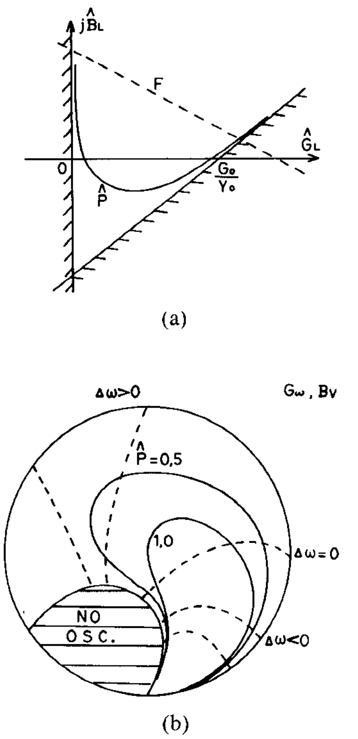

Fig. 3. Rieke diagram containing G_ω and B_v. (a) Complex load plane (b) Rieke diagram (case of $B_v < 0, G_\omega > 0$).

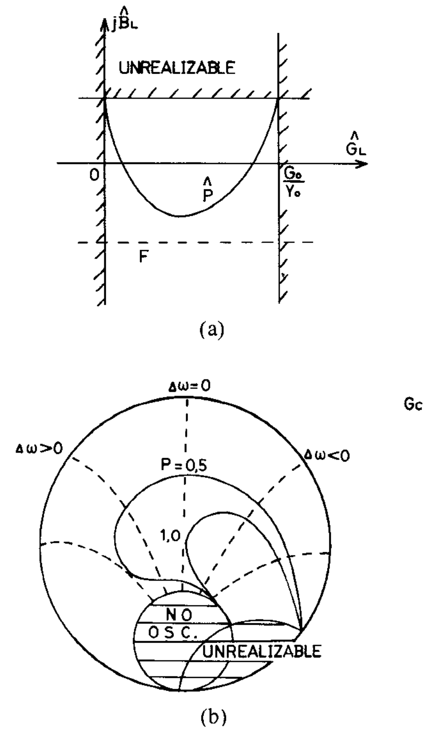

Fig. 4. Rieke diagram containing G_c. (a) Complex load plane. (b) Rieke diagram (case of $G_c > 0$).

tively given by (see Fig. 3)

$$-G_0+\left(G_V-\frac{B_VG_\omega}{B_\omega}\right)\hat{P}G_0^2/4G_V\hat{G}_LY_0 + \hat{G}_LY_0 - G_\omega\hat{B}_LY_0/B_\omega = 0 \quad (13)$$

$$\hat{B}_LY_0 + B_\omega\Delta\omega + \left(G_0 - G_\omega\Delta\omega - \hat{G}_LY_0\right)B_V/G_V = 0. \quad (14)$$

The coefficient G_ω makes the equi-power loci asymmetric with respect to frequency. The equi-frequency loci have a tendency to turn to the left toward the periphery when B_V is positive, and to the right when B_V is negative. The stability condition is obtained from (9)

$$G_VB_\omega - B_VG_\omega > 0. \quad (15)$$

2) Meaning of Coefficient G_C: Fig. 4 shows the Rieke diagram of an oscillator model containing a parameter G_C in addition to van der Pol's model (1). The equi-power loci are given by

$$\left(\hat{G}_LY_0\right)^2 - G_0\hat{G}_LY_0 + \hat{P}G_0^2\left\{G_V - G_CY_0\hat{B}_L/B_\omega\right\}/4G_V = 0. \quad (16)$$

The equi-frequency loci are given by (12). The stability condition is given by

$$G_V - G_CY_0\hat{B}_L/B_\omega > 0. \quad (17)$$

3) Meaning of Coefficient B_C: Fig. 5 shows the Rieke diagram containing B_C in addition to van der Pol's model (1). The equi-power loci are given by (11), and equi-frequency loci are obtained from

$$Y_0\hat{B}_L + \Delta\omega\left\{B_\omega + \left(G_0 - Y_0\hat{G}_L\right)B_C/G_V\right\} = 0. \quad (18)$$

The stability condition is expressed by

$$B_\omega G_V + B_C\left(G_0 - Y_0\hat{G}_L\right) > 0. \quad (19)$$

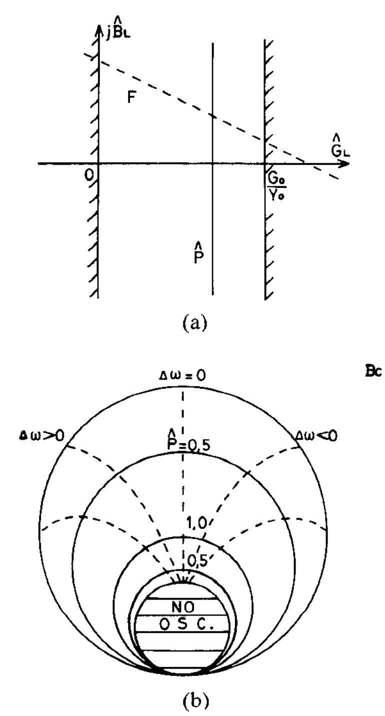

Fig. 5. Rieke diagram containing B_c. (a) Complex load plane (b) Rieke diagram (case of $B_c > 0$).

4) Meaning of Coefficient $G_{\omega 2}$: Fig. 6 shows the Rieke diagram containing $G_{\omega 2}$ in addition to van der Pol's oscillator. The maximum output power is generated at only one point. The practical oscillators have positive $G_{\omega 2}$. The equi-power loci are represented by

$$\hat{P}G_0^2/4 + \left(\hat{G}_LY_0\right)^2 - \hat{G}_LY_0\left\{G_0 - G_{\omega 2}\left(\hat{B}_LY_0/B_\omega\right)^2\right\} = 0. \quad (20)$$

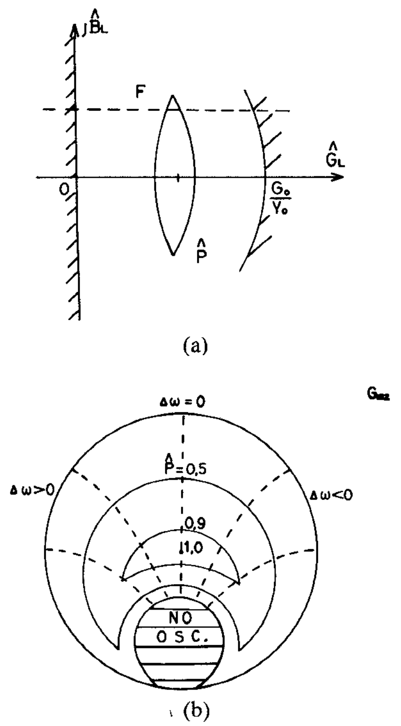

Fig. 6. Rieke diagram containing $G_{\omega 2}$. (a) Complex load plane. (b) Rieke diagram (case of $G_{\omega 2} > 0$).

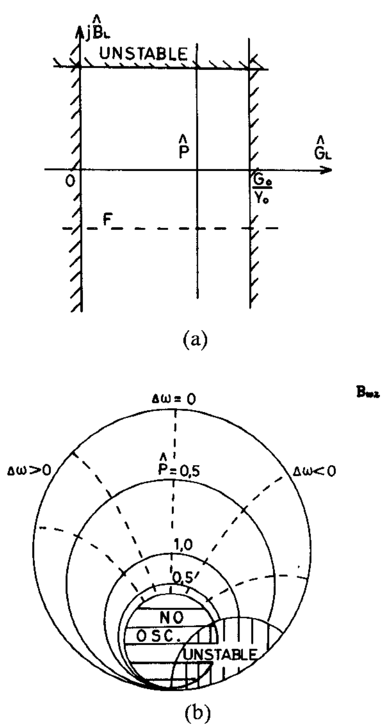

Fig. 7. Rieke diagram comtaining $B_{\omega 2}$. (a) Complex load plane. (b) Rieke diagram (case of $B_{\omega 2} < 0$).

The equi-frequency loci are given by (12). The stability condition is $G_V, B_V > 0$.

5) Meaning of coefficient $B_{\omega 2}$: Fig. 7 shows the Rieke diagram containing $B_{\omega 2}$ in addition to van der Pol's model (1). The equi-power loci are given by (12). The equi-frequency loci are represented by

$$\hat{B}_L Y_0 = -(1 + B_{\omega 2}\Delta\omega / B_\omega)\Delta\omega B_\omega. \tag{21}$$

The stability condition is

$$B_\omega + 2B_{\omega 2}\Delta\omega > 0. \tag{22}$$

III. Method to Determine the Characteristic Parameters of an Oscillator by Use of the Rieke Diagram

Let us consider how to determine the coefficients of $\Delta\omega$ and $|V|^2$ in (4) by use of the Rieke diagram. The line length shown in Fig. 1 rotates the Rieke diagram. After we rotate it to get the standardized Rieke diagram, we determine the coefficients of (4).[2]

A. The Use of the Least-Square Method

Generally speaking, five complex coefficients of (4) can be determined by five measured values. If we want to get more accurate solutions, we can make use of the least-square method. The residual of (4) from the N measured values

$$\hat{Y}_{Li} = \hat{G}_{Li} + j\hat{B}_{Li} \qquad (i = 1 \sim N)$$

is written as

$$R_i = \hat{Y}(j\omega_i, P_i/G_{Li}) + \hat{Y}_{Li} \qquad (i = 1 \sim N). \tag{23}$$

From the definition of the least-square method, the coefficients

[2]The standard diagram, in the case of van der Pol's oscillator, is such that the center frequency line ($\Delta\omega = 0$) is equal to the load line of zero susceptance and nonoscillation region exists in the heavy-load-admittance region.

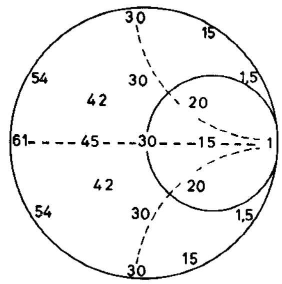

Fig. 8. Distribution of weight.

are determined by minimizing S_R

$$S_R = \sum_{i=1}^{N} \{\mathrm{Re}(R_i)\}^2 + \sum_{i=1}^{N} \{\mathrm{Im}(R_i)\}^2. \tag{24}$$

B. Weighted Averaging Method

The Smith chart is not uniform with respect to the density of admittance. This leads to nonuniform accuracy of the result according to the feature of the Smith chart. To rectify it, we adopt a weighting function. Let us assume a weighting function[3]

$$W(|\Gamma|, \theta) = 30.5 - 29.5|\Gamma|\cos\theta \tag{25}$$

the distribution of weight of which is shown in Fig. 8. The left part of the Smith chart (small admittance region) has heavier weight than the right part, so that the relative accuracy is averaged on the Smith chart. With the weighting function (25) employed, (24) is modified as

$$S_{RW} = \sum_{i=1}^{N} \{\mathrm{Re}(R_i)\}^2 W_i + \sum_{i=1}^{N} \{\mathrm{Im}(R_i)\}^2 W_i. \tag{26}$$

[3]Since there is no definite rule to find the weighting function, (25) has been assumed in an intuitive and empirical manner.

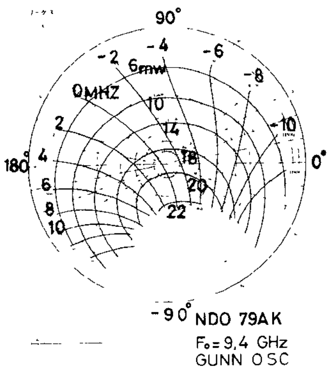

(a)

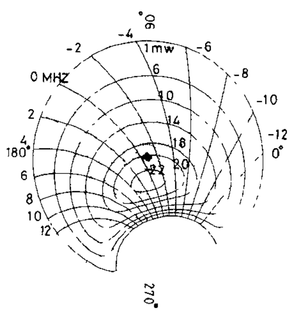

(b)

Fig. 9. Example of a Gunn oscillator ND079AK. (a) Measured Rieke diagram. (b) Reproduced Rieke diagram.

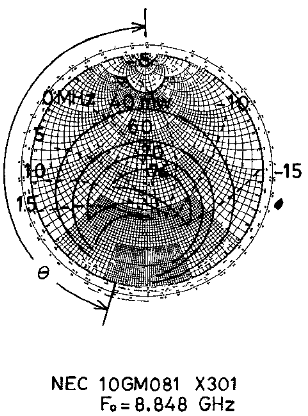

(a)

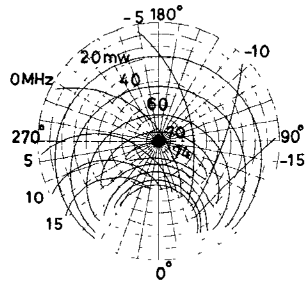

(b)

Fig. 10. Example of a Gunn oscillator 10GM081. (a) Measured Rieke diagram. (b) Reproduced Rieke diagram.

By solving the partial differential equation, we can obtain the coefficients of (4) (see Appendix II).

IV. Examples

By use of the method described above, let us determine the admittances of practical oscillators. As an example, Fig. 9(a) shows the Rieke diagram of a Gunn oscillator ND079AK. The values of the parameters shown in Table I were determined from 16 measured points on the Rieke diagram. Fig. 9(b) shows the calculated Rieke diagram using the values of this table. Comparing Fig. 9(a) with (b), we see a good agreement between them, and by far a better agreement than with van der Pol's model.

Fig. 10 shows another example of a Gunn oscillator 10GM081. The relation among (a), (b), and Table II is the same as that of Fig. 9. Figs. 10(a) and (b) show a good overall agreement in between.

TABLE I
Coefficients for Fig. 9(a)+(b)

$G_0=0.592\times10^{-2}$	$B_0=-0.991\times10^{-3}$
$G_\omega=-0.861\times10^{-4}$	$B_\omega=0.357\times10^{-3}$
$G_V=0.387\times10^{-6}$	$B_V=0.118\times10^{-6}$
$G_C=0.955\times10^{-8}$	$B_C=-0.890\times10^{-8}$
$G_{\omega 2}=0.882\times10^{-5}$	$B_{\omega 2}=0.764\times10^{-6}$

POWER(mw)
FREQ. $\Delta\omega$ (MHZ)
LINE ADM. 0.002(℧)

TABLE II
Coefficients for Fig. 10(a)+(b)

$G_0=0.00471$	$B_0=-0.00240$
$G_\omega=-0.549\times10^{-4}$	$B_\omega=0.147\times10^{-3}$
$G_V=0.735\times10^{-7}$	$B_V=0.572\times10^{-7}$
$G_C=0.169\times10^{-8}$	$B_C=0.187\times10^{-8}$
$G_{\omega 2}=0.542\times10^{-6}$	$B_{\omega 2}=0.196\times10^{-5}$

LINE ADM. 0.002[℧]
FREQ. MHz
POWER mw

V. Conclusion

We attempted to represent the admittance of oscillators in terms of mathematical formulas, whose parameters are determined from the Rieke diagram. As a result, we found that (4) is sufficient to represent the characteristics of ordinary microwave oscillators. With this formula applied to computer analysis, the design of oscillator circuits and the drawing of the Rieke diagram will be made easier.

Acknowledgment

The authors would like to thank Dr. H. Yamamoto, Dr. M. Akaike, and E. Hagiwara for their interest. H. Mizuno of the Nippon Denso Co., Ltd., made his experimental results available to us.

Appendix I
Equi-Power Loci of van der Pol's Oscillator

Equation (1) represents the characteristics of van der Pol's oscillator. Connecting a load Y_L to the oscillator leads to (5). The real part of (5) is

$$-G_0+G_V|V|^2+G_L=0. \tag{A1}$$

Substuting (10) into (A1), we have

$$G_L^2-G_0G_L+G_0^2\hat{P}/4=0. \tag{A2}$$

The equi-power loci are plotted using (A2). The maximum output power $\hat{P}=4G_VP_m/G_0^2=1$ is generated when $\hat{G}_L=G_0/2Y_0$.

Appendix II
Method to Determine the Coefficients by Use of the Least-Square Method

The minimization of (26) is attained by minimizing both the real and imaginary parts of (26). Setting

$$g \equiv \mathrm{Im}\{S_{RW}\} \qquad f \equiv \mathrm{Re}\{S_{RW}\}$$

we have the minimization conditions

$$\frac{\partial f}{\partial G_0}=0, \frac{\partial f}{\partial G_\omega}=0, \frac{\partial f}{\partial G_V}=0, \frac{\partial f}{\partial G_C}=0, \frac{\partial f}{\partial G_{\omega 2}}=0 \qquad \text{(A3)}$$

$$\frac{\partial g}{\partial B_0}=0, \frac{\partial g}{\partial B_\omega}=0, \frac{\partial g}{\partial B_V}=0, \frac{\partial g}{\partial B_C}=0, \frac{\partial g}{\partial B_{\omega 2}}=0. \qquad \text{(A4)}$$

We find the coefficients of (4) by solving the simultaneous equations (A3) and (A4).

References

[1] D R. Hamilton, J. K. Knipp, and J. B. H. Kuper, *Klystron and Microwave Triodes*. New York: McGraw-Hill, Radiation Laboratory Series, 1948, pp. 404–440.

[2] J. R. Pierce and W. G. Shepherd, "Reflex oscillators," *Bell Syst. Tech. J.*, vol. 26, no. 3, pp. 460–681, 1947.

[3] M. Nakajima and J. Ikenoue, "Locking phenomena in microwave oscillator circuits," *Int. J. Electron.*, vol. 44, pp. 465–472, 1978.

[4] T. Hirota, M. Nakajima, and J. Ikenoue, "A simple equivalent circuit of a microstrip oscillator allowing for nonlinearity," *Int. J. Electron.*, vol. 48, pp. 427–434, 1980.

Single-Mode Fiber Design for Minimum Dispersion

PAULO SÉRGIO MOTTA PIRES and DAVID ANTHONY ROGERS, MEMBER, IEEE

***Abstract*—The value of the radius of the core of a single-mode step-index optical fiber for minimum dispersion is calculated with the normalized frequency in the range $1.0 \leqslant V \leqslant 2.5$, using the approximation for the eigenvalue U proposed by Miyagi and Nishida [1]. This calculation is made by solving the total dispersion equation for the core radius when the wavelength assigned is assumed to be that necessary for minimum total dispersion. The computational procedure presented is simple enough to be accomplished on a programmable calculator or microcomputer. This work makes possible the characterization, with reasonable precision, of the ideal fiber that should be used with the available optical source.**

I. Introduction

The bandwidth for single-mode optical fibers is maximum when operation of the system takes place at the wavelength for minimum total dispersion $\hat{\lambda}$. Theoretical research concerning dispersion in monomodal step-index optical fibers has been based on the assumed prior knowledge of the core radius and of the materials that constitute the core and the cladding, so that the wavelength $\hat{\lambda}$ can be found. Since the wavelength is established by the characteristics of the known fiber, the next step is to search for the corresponding optical source.

Manuscript received January 14, 1982; revised June 15, 1983. The work of P. S. M. Pires was partially supported by the Conselho Nacional de Desenvolvimento Científico e Technológico (CNPq), Brazil.

P. S. M. Pires is on leave from the Department of Electrical Engineering, Universidade Federal do Rio Grande do Norte, 59.000 Natal, RN, Brazil, doing his doctoral studies at the Universidade Estadual de Campinas (UNICAMP), Caixa Postal 6125, 13.100-Campinas, S. P., Brazil.

D. A. Rogers is with the Department of Electrical and Electronics Engineering, North Dakota State University, Fargo, ND 58105.

In previous publications [2], [3], the exact characteristic equations and numerical methods for differentiation and interpolation for calculating the value of $\hat{\lambda}$ for monomodal step-index optical fibers have been used. The results thus obtained were compared with those that were arrived at utilizing asymptotic formulas [4]–[7]. In spite of the excellent results obtained, even in the asymptotic limit, and having made possible the extension of the analysis that had been developed to other cases, the large quantity of calculations required the availability of medium to large computer systems. When such systems are not available, some approximate methods, with acceptable precision in these circumstances, allow the implementation of programs to calculate the value of $\hat{\lambda}$ using programmable calculators or microcomputer systems.

Utilizing the total dispersion formula established by South [7], derived with the objective of calculating $\hat{\lambda}$, together with the approximate formulation for the eigenfunction U proposed by Miyagi and Nishida [1], we prepared some programs for the TI-59 programmable calculator that make possible the design of monomodal step-index optical fibers. With the utilization of these programs, we obtain the value of the radius of the core, within the normalized frequency range $1.0 \leqslant V \leqslant 2.5$, for any value of the wavelength assumed to be that for minimum dispersion. In other words, we start with knowledge of the materials that will constitute the core and the cladding and with the value of the wavelength, and subsequently calculate the value of the core radius for which maximum information transfer will occur. Thus we have the possibility of characterizing with reasonable precision [8] the ideal optical fiber for use with the available source.

In Section II, we present the equations used, while in Section III, we will describe the computational methods implemented. In Section IV, we present some values of the core radii $\hat{a}$ for information transmission at minimum dispersion and some curves obtained for hypothetical fibers.

II. Formulation of the Problem

The value of the wavelength for minimum total dispersion $\hat{\lambda}$ depends on: a) the physical characteristics of the materials that constitute the core and the cladding, b) the core radius, and c) the propagation constant of the dominant HE_{11} mode and some of its derivatives. This value is calculated for the core radius a, with a predetermined value (for a known fiber) by solving the total dispersion equation [7]

$$D_T(a) = -\frac{\lambda}{cn_e}\left[(1-b)\nu_2 + b\nu_1 + 2b'\phi + \frac{1}{2}b''\theta - \frac{1}{n_e^2}\left(n_2 n_2' + b\phi + \frac{1}{2}b'\theta\right)^2\right]\Big|_{\lambda=\hat{\lambda}} = 0 \qquad (1)$$

where c is the phase velocity in a vacuum, λ is the wavelength in free space

$$\nu_j = n_j n_j'' + (n_j')^2, \qquad j = 1,2 \qquad \text{(2a)}$$

$$\phi = n_1 n_1' - n_2 n_2' \qquad \text{(2b)}$$

$$\theta = n_1^2 - n_2^2, \qquad n_e^2 = n_2^2 + b\theta. \qquad \text{(2c)}$$

The primes and double primes in (1) and (2) represent differentiations with respect to the wavelength λ. In (2a)–(2c), n_1 and n_2 represent the refractive indices of the core and cladding, respectively. In this paper, we will assume that the wavelength depen-